Electronic Supplementary Information

Radio frequency alternating electromagnetic field enhanced tetraruthenium polyoxometalate electrocatalytic water oxidation

Shuntaro Tsubaki *[a], Shogo Hayakawa [a], Tadaharu Ueda [b], Satoshi Fujii [ac], Jie Zhang [d], Alan Bond [d], and Yuji Wada [d]

[a] School of Materials and Chemical Technology Tokyo Institute of Technology, Ookayama 2-12-1 E4-3, Meguro, Tokyo, 152-8550, Japan

[b] Department of Information and Communication Systems Engineering, Okinawa National College of Technology, 905 Henoko, Nago-shi, Okinawa 905-2192, Japan

[c] Department of Marine Resource Science, Faculty of Agriculture and Marine Science, Kochi University, Monobe-otsu 200, Nankoku, 783-8502, Japan

[d] School of Chemistry, Monash University, Clayton, Victoria 3800, Australia

(1) Synthesis and characterization of protonated and deuterated Ru-POMs.
(2) Evaluation of uncompensated resistance.
(3) Details of the radio frequency (RF) reaction system.
(4) Enhancement of oxidation current density in the absence and presence of H_xRu-POMs.
(5) Temperature changes accompanying the electrochemical water oxidation under pulsed RF.

(1) Synthesis and characterization of protonated and deuterated tetraruthenium-polyoxometalates (Ru-POMs).

Tetraruthenium-polyoxotungstate ($[Ru_4(\mu\text{-}O)_4(\mu\text{-}OH)_2(H_2O)_4(\gamma\text{-}SiW_{10}O_{36})_2]^{10-}$: Ru-POM), which contains $\{Ru_4O_4(OH)_2(H_2O)_4\}^{6+}$ sandwiched by two $[\gamma\text{-}SiW_{10}O_{36}]^{8-}$ unit was synthesized according to a reported method. [14] Thus, $K_8[\beta_2\text{-}SiW_{11}O_{39}]$ was synthesized and converted to $K_8[\gamma\text{-}SiW_{10}O_{36}]$. Upon addition of $RuCl_3$, $Rb_8K_2[\{Ru_4O_4(OH)_2(H_2O)_4\}(\gamma\text{-}SiW_{10}O_{36})_2]$ was obtained. Ru-POM was characterized by ATR FT-IR spectra (Fig. S1A). Electrochemical characterization of Ru-POM was undertaken by cyclic voltammetry in a three-electrode cell using glassy carbon as the working electrode with 0.1 M HCl added as supporting electrolyte. IR absorptions as well as mid-point potentials (E_m) and peak-to-peak separations ($\Delta E\mathrm{p}^{\mathrm{ref}}$) obtained from cyclic voltammogram were in good agreement with literature reports (Table S1). [14]

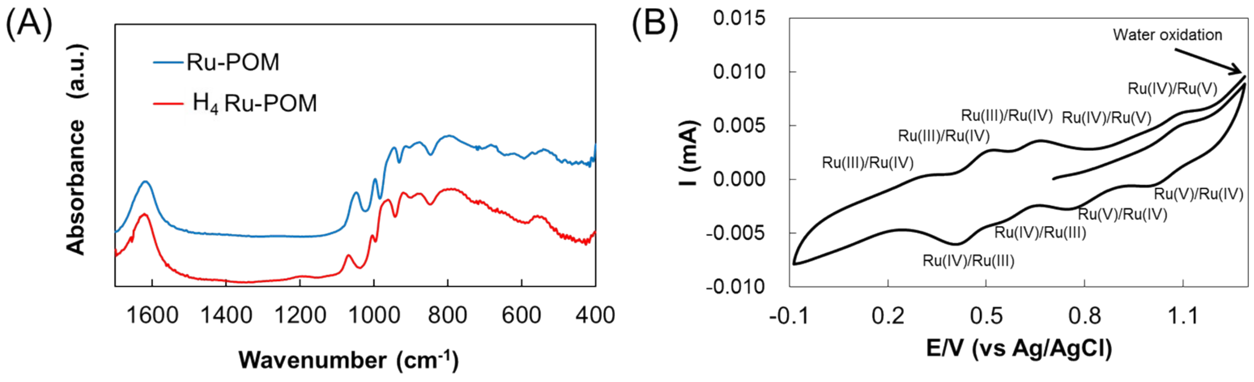

Figure S1. Characterizations of Ru-POM and H_4Ru-POM by (A) FT-IR and (B) cyclic voltammetry: Ru-POM (1 mM); supporting electrolyte, 0.1 M HCl; working electrode, glassy carbon; reference electrode, Ag/AgCl (saturated KCl); counter electrode, Pt wire; potential range, $E_{\mathrm{start}} = 0.705$ V vs Ag/AgCl, $E_{\mathrm{switch}} = 1.288$ and -0.087 V vs Ag/AgCl, scan rate, 25 mV s^{-1}.

Table S1. Mid-point potentials (E_m vs Ag/AgCl) and peak-to-peak separations (ΔE_p) obtained by cyclic voltammetry of Ru-POM under conditions given in caption to Figure S1.

Process	This study		Reference [14]	
	E_m (mV)	ΔE_p (mV)	E_m (mV)	ΔE_p (mV)
Ru(IV)/Ru(V)	1036	108	1028	85
Ru(IV)/Ru(V)	856	220	860	161
Ru(III)/Ru(IV)	612	89	596	90
Ru(III)/Ru(IV)	454	97	440	93

*$E_m = (E_c + E_a)/2$ where E_c and E_p are cathodic and anodic peak potentials, respectively.

H_xRu-POM was prepared by reaction of the cation exchange resin (DOWEX™ 50W×8, 100-200 mesh, H^+-form) at molar ratios of 0.8, 1.2, 1.6 and 2.0 with Ru-POM for 3 days (Fig. S2). The degree of substitution by H^+ was determined to be 4, 6, 8, 9 by ICP-OES (Table S2). The structure of H_4Ru-POM was confirmed to be the same as Ru-POM by FT-IR (Fig. S1A) as well as electrochemical oxidation properties analyzed by linear sweep voltammetry (Fig. S5).

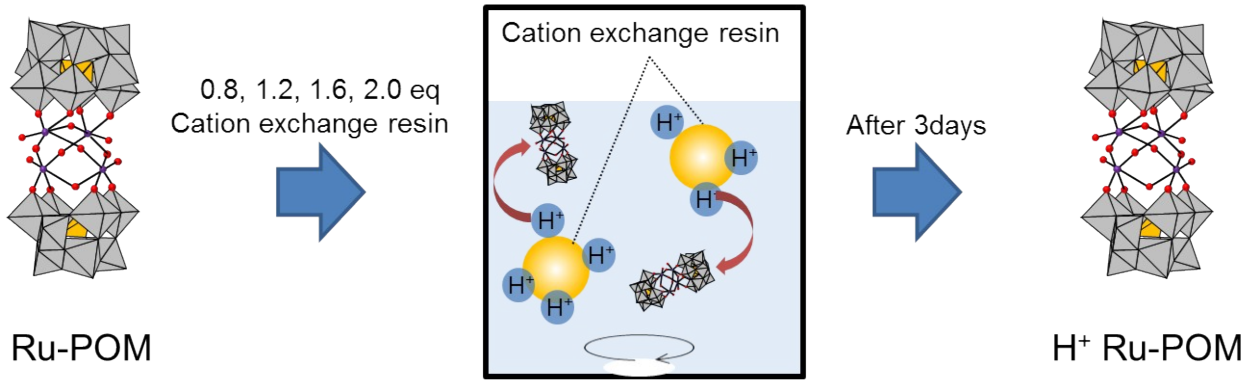

Figure S2 Schematic illustration of the preparation of H_xRu-POMs with different levels of proton substitution.

Table S2 Ratio of H^+ and Ru-POMs in H_xRu-POM samples.

Sample	Rb	K	Na	Ru	Si	W
Theoretical	8	2	-	4	2	20
Ru-POM	8.8	1.4	-	4.0	2.1	20.0
H_4Ru-POM	4.6	1.0	-	3.9	2.1	20.0
H_6Ru-POM	3.1	0.6	-	4.3	2.1	20.0
H_8Ru-POM	1.9	0.3	-	4.2	2.1	20.0
H_9Ru-POM	1.1	0.3	-	4.0	1.9	20.0
D_8Ru-POM	1.4	0.3	0.7	4.2	2.0	20.0

Deuterated Ru-POM was synthesized by addition of deuterium substituted cation-exchange resin (DOWEX™ HCR-S, Na^+-form) which had been prepared by DCl-treatment of the cation-exchange resin (Fig. S3). A two molar equivalent of deuterated cation exchange resin was added to the Ru-POM solution and left to react for 3 days. The level of D^+ substitution was determined to be 8 by ICP-OES (Table S2). The small amount of Na^+ present was derived from use of the Na^+-form cation exchange resin used in as the starting material.

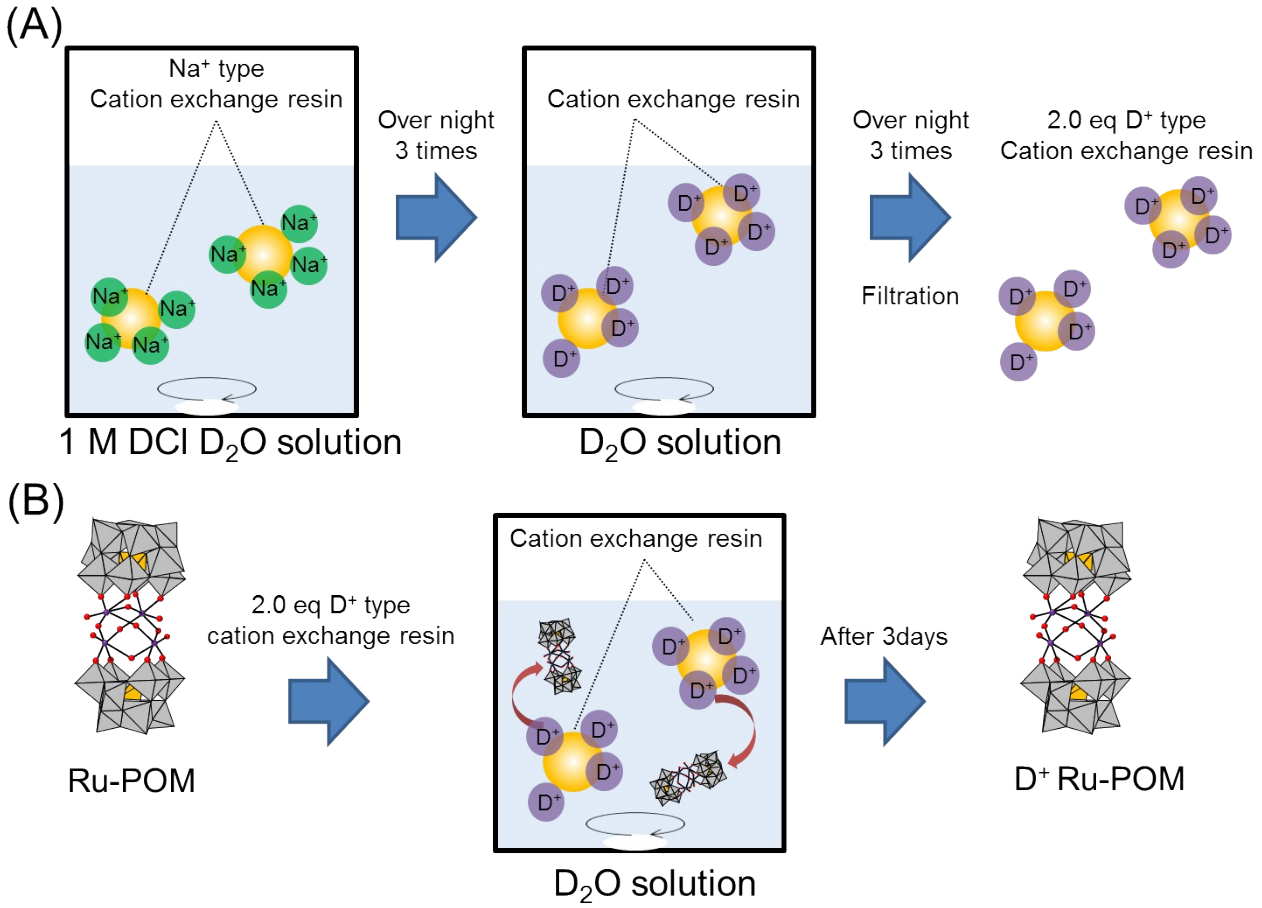

Figure S3. Schematic illustration of the preparation of deuterated Ru-POM. (A) Preparation of deuterated cation exchanger resin. (B) Deuteration of Ru-POM.

(2) Evaluation of uncompensated resistance

Supporting electrolyte other than that provided by the POM was not present in electrochemical reactions under MW and RF in order to minimize interaction between the applied electromagnetic field and electrolyte due to ionic conduction. The resistances of the POM solutions and uncompensated resistance present in the electrochemical apparatus were evaluated by dielectric measurement and electrochemical impedance spectroscopy, respectively.

The resistance of the 5 mM of H_xRu-POM solution was determined by the coaxial probe method using the Cole–Cole model. [6]

$$\varepsilon_r^* = \varepsilon_\infty + \frac{\varepsilon_s - \varepsilon_\infty}{1 + (j\omega\tau)^\beta} - \frac{j\sigma}{\omega\varepsilon_0} \tag{1}$$

where, ε^*, ε_0, ε_s, ε_∞, j, ω, τ, and σ are the complex permittivity, permittivity of free space, the permittivity at a static frequency, the permittivity at infinite frequency, the imaginary unit, angular frequency, relaxation time, conductivity of the electrolyte, respectively. The conductivities of H_xRu-POM determined via this method are summarized in Table S3. As expected, the conductivity of the H_xRu-POM increased linearly with the level of protonation. H_9Ru-POM (5 mM) has a similar conductivity to NaCl (100 mM). The conductivity values converted to resistance ones are as also provided in Table S3.

Table S3. The conductivities and pH of H_xRu-POM.

HxRu-POM	Concentration (mM)	pH	Conductivity (mS/m)	Resistance (Ω·m)
Ru-POM	5	2.8	297	3.37
H_4Ru-POM	5	1.8	489	2.05
H_6Ru-POM	5	1.8	666	1.50
H_8Ru-POM	5	1.5	756	1.32
H_9Ru-POM	5	1.5	939	1.07
D_8Ru-POM	5		572	1.75
NaCl	100		912	1.10
$MgSO_4$	100		825	1.21

The series resistance (R_s) associated with the electrolyte solution, salt bridge and distance separation of electrodes was estimated using electrochemical impedance spectroscopy (EIS, Biologic, SP-200) in the same cell as the RF experiments (2 compartments connected by a salt bridge). Fig. S4 shows the equivalent circuit used for estimating Rs.

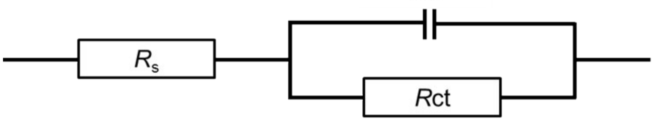

Figure S4. The equivalent circuit used for evaluation of R_s of the electrochemical system. R_s = series resistance, C_{dl} = double layer capacitance, R_{ct} = charge transfer resistance.

The inverse of the impedance (*Z*) of the RC parallel circuit is given by equation (2):

$$\frac{1}{Z} = \frac{1}{Z_{Rct}} + \frac{1}{Z_{Cdl}} \tag{2}$$

It therefore follows that the impedance is given by equation (3).

$$Z = \frac{Z_{Rct} Z_{Cdl}}{Z_{Rct} + Z_{Cdl}} \tag{3}$$

The total impedance of the equivalent circuit (Z_{total}) is the sum of the impedance of the series resistance (Z_{Rs}), impedance of the resistance (Z_R) and impedance of the capacitance component (Z_c) as in equation (4) to (6).

$$Z_{total} = Z_{Rs} + \frac{Z_R Z_C}{Z_R + Z_C} \tag{4}$$

$$Z_R = R_{ct} \tag{5}$$

$$Z_C = \frac{1}{j\omega C_{dl}} \tag{6}$$

Since Z_c is much less than the Z_R at high frequency, Z_{total} at high frequency become equal to R_s. With these assumptions, R_s can be obtained by measuring the impedance in the high frequency range. The R_s values are listed in Table S4.

Table S4. Series resistance (R_s) of the electrochemical system.

Sample	R_s (Ω)
Ru-POM	1683 ± 3
H_4Ru-POM	1611 ± 1
H_6Ru-POM	1966 ± 1
H_8Ru-POM	1609 ± 5
H_9Ru-POM	1547 ± 1

The effective applied potentials *E* (vs RHE) when potentials of 1.2 V, 1.6 V, and 2.0 V vs Ag/AgCl were used, as summarized in Table S5, were estimated from equation (7).

$$E\ (V\ vs\ RHE) = E_{Ag/AgCl(in\ KCl)} + E_{ref.} + \frac{RT}{F} pH - I\,Rs \tag{7}$$

where, E_{ref} (sat. KCl) and *I* are the potential of the reference electrode (0.199 V vs RHE) and current magnitude when 1.2 V, 1.6 V and 2.0 V vs Ag/AgCl was applied, respectively. The raw and corrected LSV are provided in Fig. S5.

Table S5. The effective potentials *E* (vs RHE) for applied potentials of 1.2 V, 1.6 V, and 2.0 V vs Ag/AgCl.

Sample (5 mM)	1.2 V vs Ag/AgCl	1.6 V vs Ag/AgCl	2.0 V vs Ag/AgCl
Ru-POM	1.49 V vs RHE	1.64 V vs RHE	1.69 V vs RHE
H_4Ru-POM	1.42 V vs RHE	1.64 V vs RHE	1.74 V vs RHE
H_6Ru-POM	1.37 V vs RHE	1.65 V vs RHE	1.75 V vs RHE
H_8Ru-POM	1.37 V vs RHE	1.64 V vs RHE	1.71 V vs RHE
H_9Ru-POM	1.41 V vs RHE	1.67 V vs RHE	1.78 V vs RHE

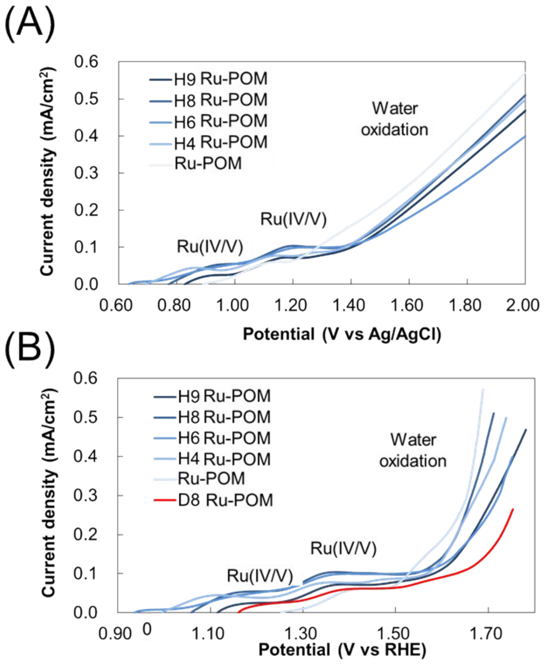

Figure S5. Linear sweep voltammograms of H_xRu-POM and D_8Ru-POM electrolyte solutions. (A) Raw data (vs Ag/AgCl) and (B) corrected data (vs RHE).

(3) Details of the radio frequency (RF) reaction system

The RF system (200 MHz) consisted of a signal generator (Keysight 8648C), a RF amplifier (Mini-Circuits, ZHL-100W-GAN+, 20-500 MHz) and a parallel plate applicator (Fuji Electronic Ind. Co. 200 MHz, Fig. S6A). The applied RF power was monitored by a power sensor (MA2481A, Anritsu Co.) and a power meter (ML2438A, Anritsu Co.) connected to a dual directional coupler (C50-108-481/4N, Pulsar Microwave Co.). The parallel applicator and matching circuits are provided in Fig. S6B.

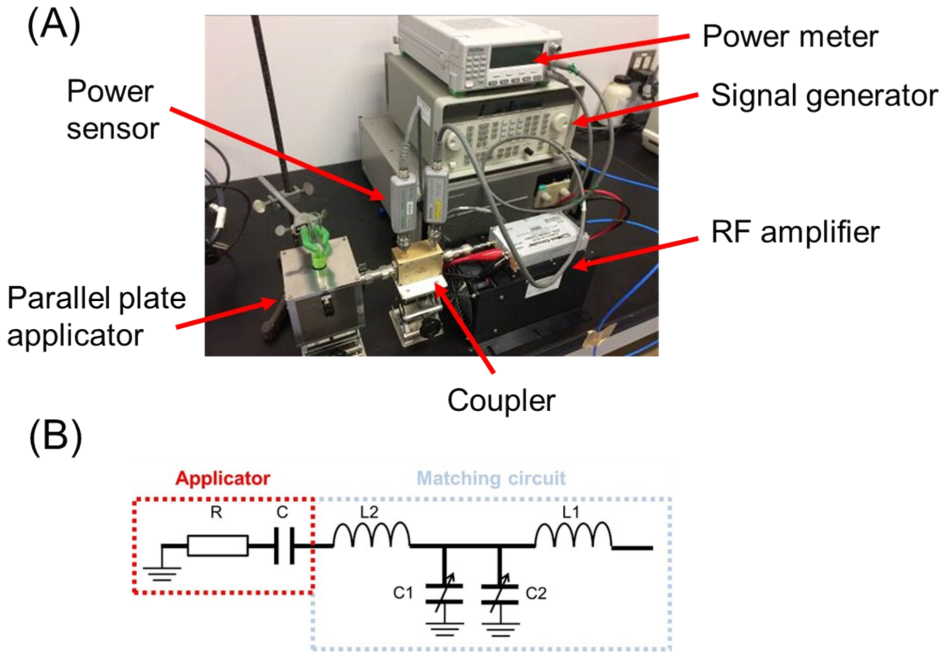

Figure S6 (A) Photograph for RF system (200 MHz) and (B) circuit diagram for parallel plate applicator and matching circuit.

(4) Enhancement of oxidation current density in the absence and presence of H_xRu-POMs

Light blue areas in Figs. S7-S12 indicate the duration of the applied RF.

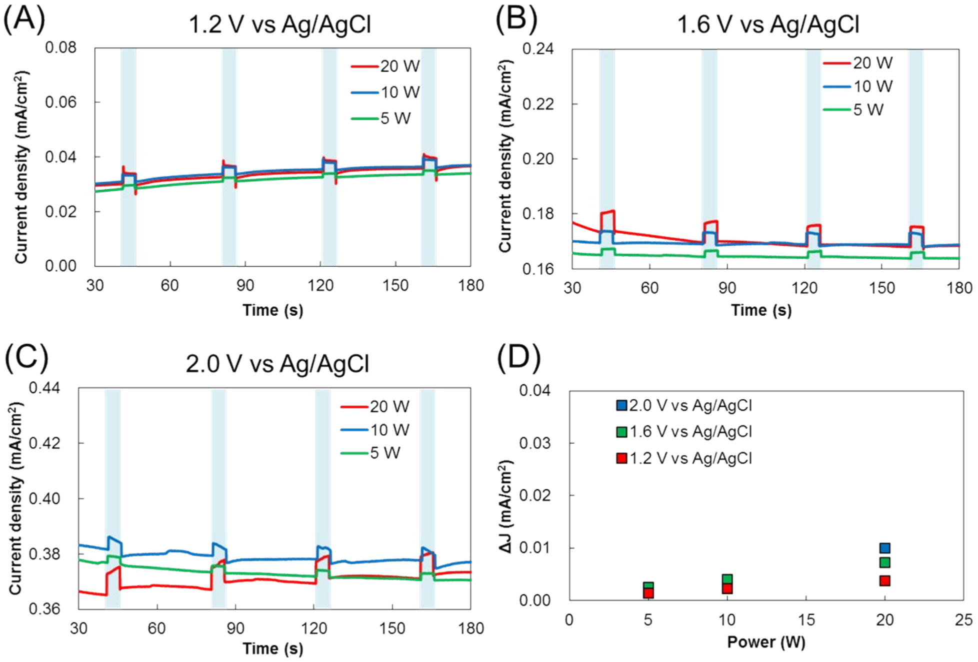

Figure S7. The Ru-POM responses to applied RF. (A-C) The oxidation current obtained during pulsed RF (5 – 20 W) at 1.2 to 2.0 V vs Ag/AgCl. (D) Increment in oxidation current density as a function of applied RF power.

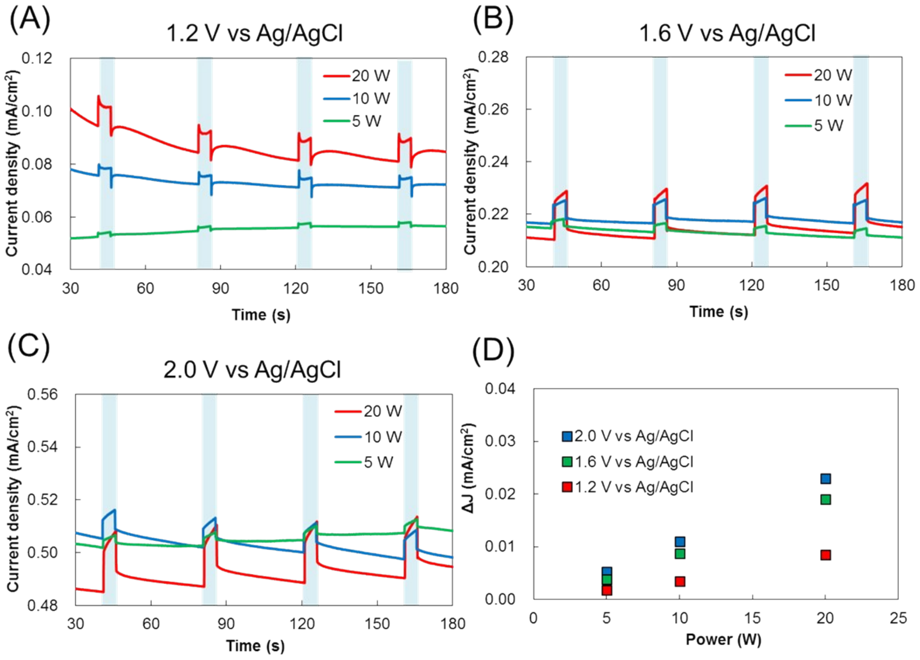

Figure S8. The H_4Ru-POM response to applied RF. (A-C) The oxidation current obtained during pulsed RF (5 – 20 W) at 1.2 to 2.0 V vs Ag/AgCl. (D) Increment in oxidation current density as a function of applied RF power.

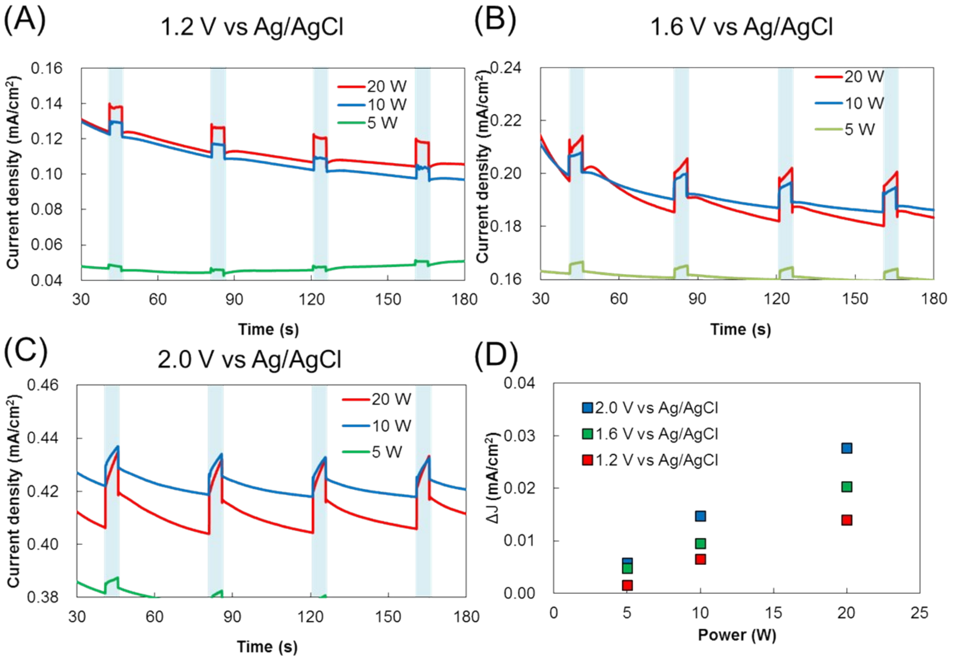

Figure S9. The H_6Ru-POM response to applied RF. (A-C) The oxidation current obtained during pulsed RF (5 – 20 W) at 1.2 to 2.0 V vs Ag/AgCl. (D) Increment in oxidation current density as a function of applied RF power.

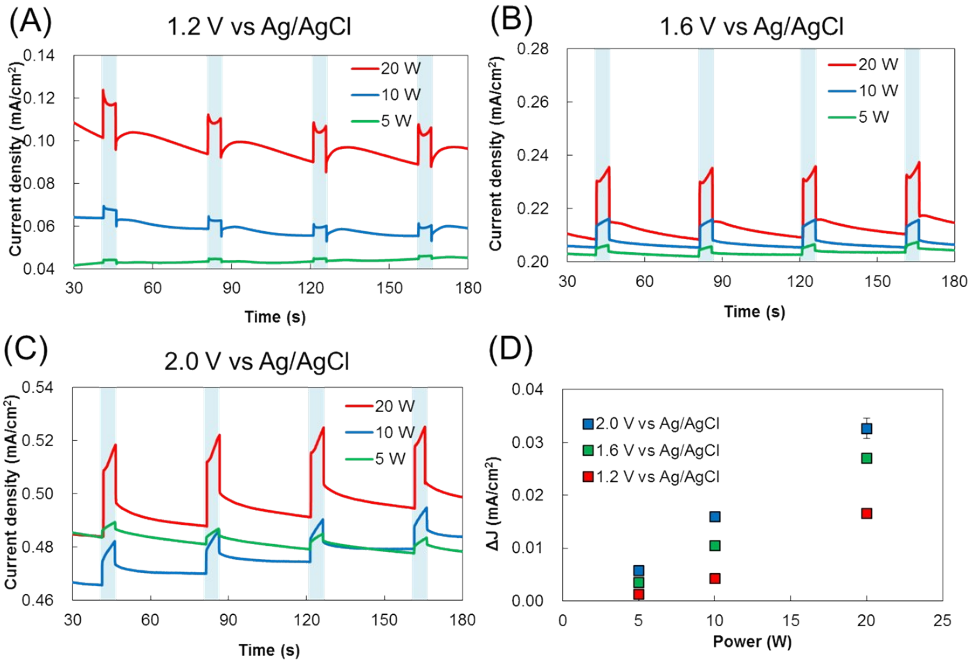

Figure S10. The H_8Ru-POM response to applied RF. (A-C) The oxidation current obtained during pulsed RF (5 – 20 W) at 1.2 to 2.0 V vs Ag/AgCl. (D) Increment in oxidation current density as a function of applied RF power.

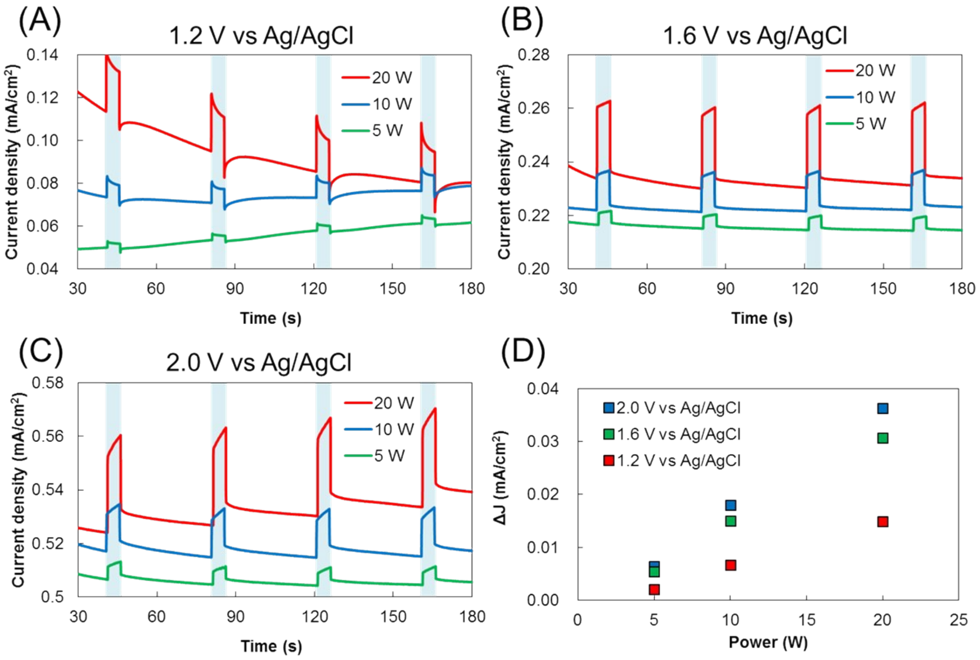

Figure S11. The H_9Ru-POM response to applied RF. (A-C) The oxidation current obtained during pulsed RF (5 – 20 W) at 1.2 to 2.0 V vs Ag/AgCl. (D) Increment in oxidation current density as a function of applied RF power.

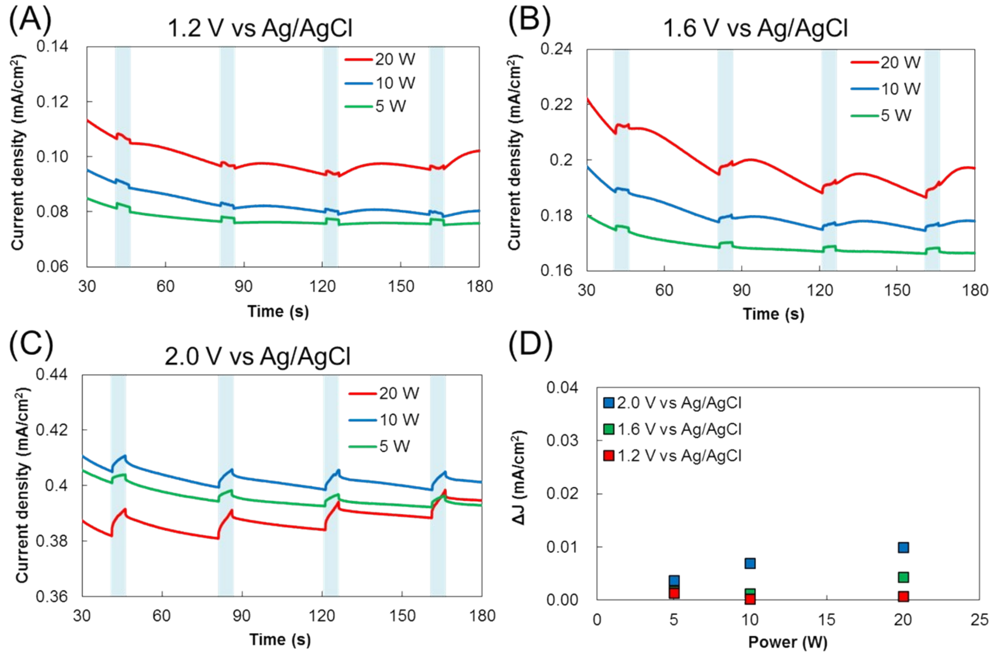

Figure S12. The D_8Ru-POM response to applied RF. (A-C) The oxidation current obtained during pulsed RF (5 – 20 W) at 1.2 to 2.0 V vs Ag/AgCl. (D) Increment in oxidation current density as a function of applied RF power.

(5) Temperature changes accompanying the electrochemical water oxidation under pulsed RF.

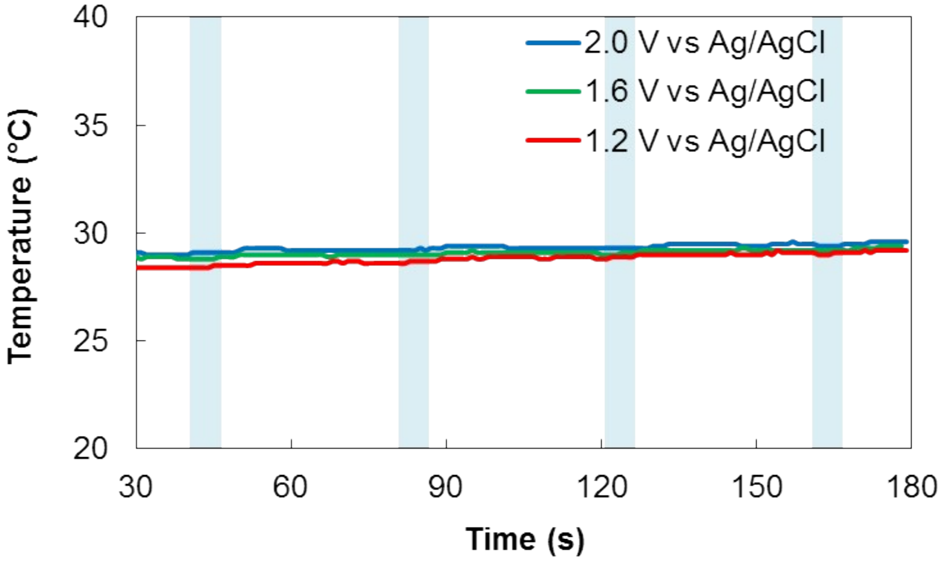

Figure S13. Temperature during application of pulsed MW (2,450 MHz) at 20 W with 5 mM Ru-POM.

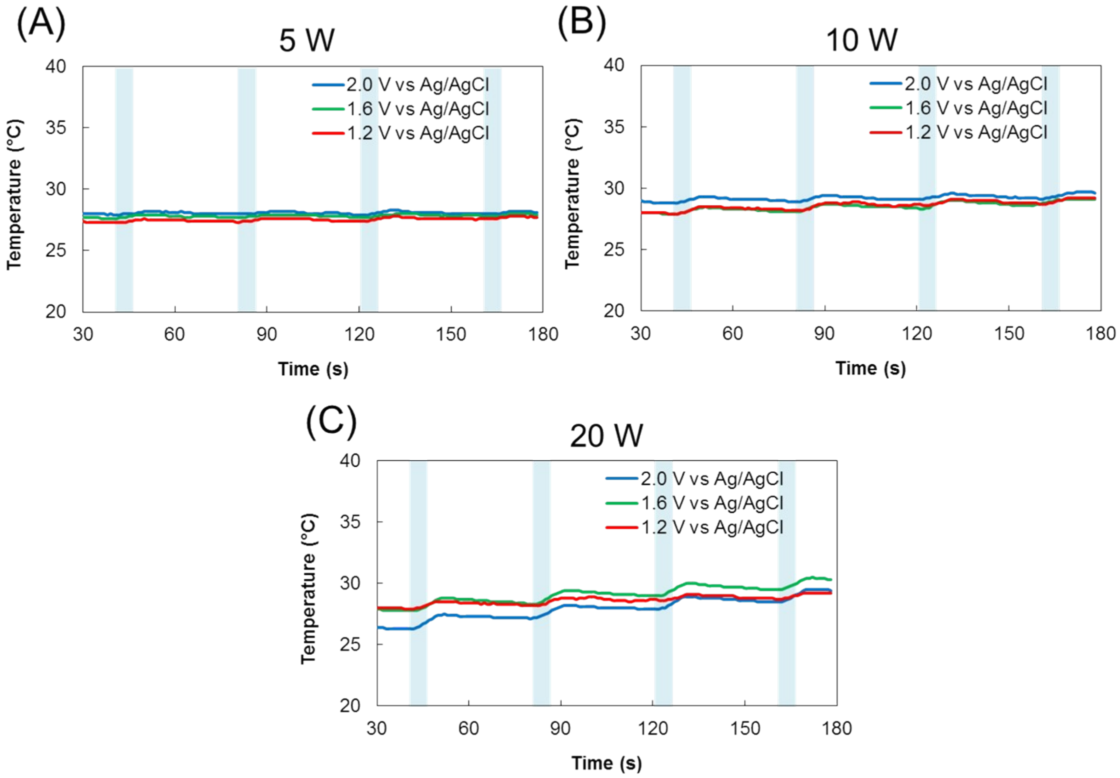

Figure S14. Temperature during application of pulsed RF with 5 mM H_4Ru-POM at (A) 5 W, (B) 10 W and (C) 20 W using designated applied potential of 1.2 to 2.0 V vs Ag/AgCl.

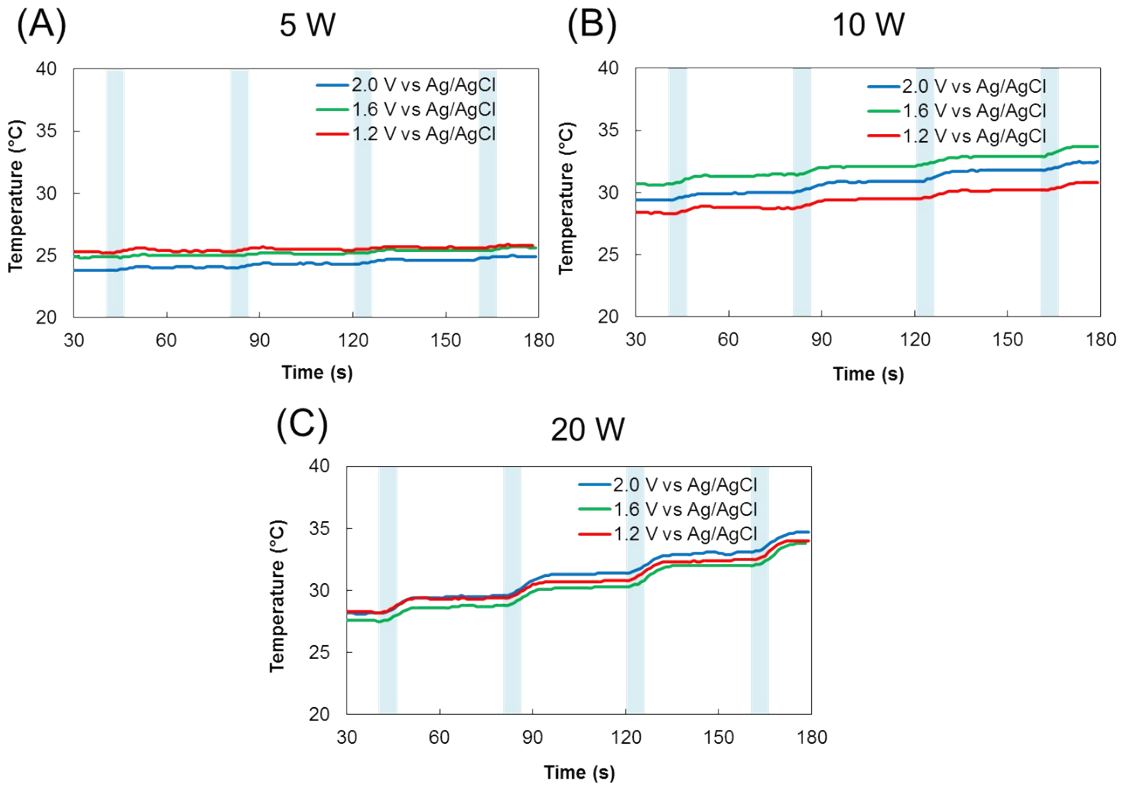

Figure S15. Temperature during application of pulsed RF with 5 mM H_6Ru-POM at (A) 5 W, (B) 10 W and (C) 20 W using designated applied potential of 1.2 to 2.0 V vs Ag/AgCl.

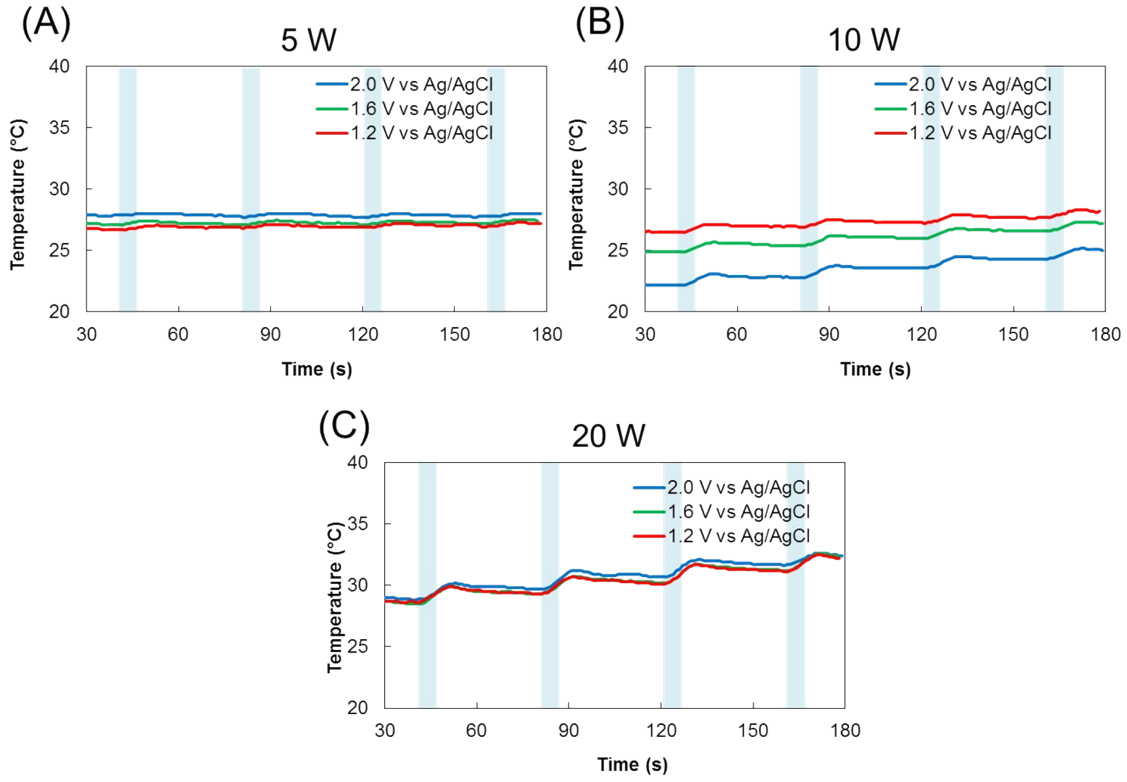

Figure S16. Temperature during application of pulsed RF using 5 mM H_8Ru-POM at (A) 5 W, (B) 10 W and (C) 20 W using designated applied potentials of 1.2 to 2.0 V vs Ag/AgCl.

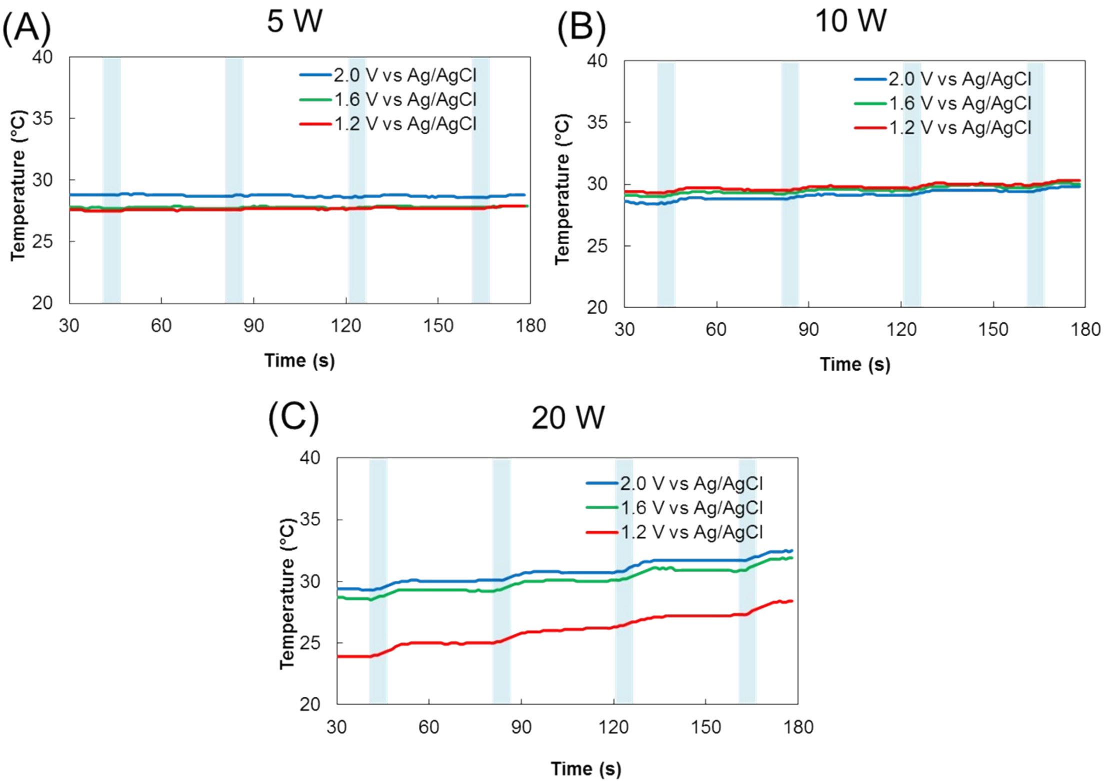

Figure S17. Temperature during application of pulsed RF with 5 mM H_9Ru-POM at (A) 5 W, (B) 10 W and (C) 20 W at applied potentials of 1.2 to 2.0 V vs Ag/AgCl.

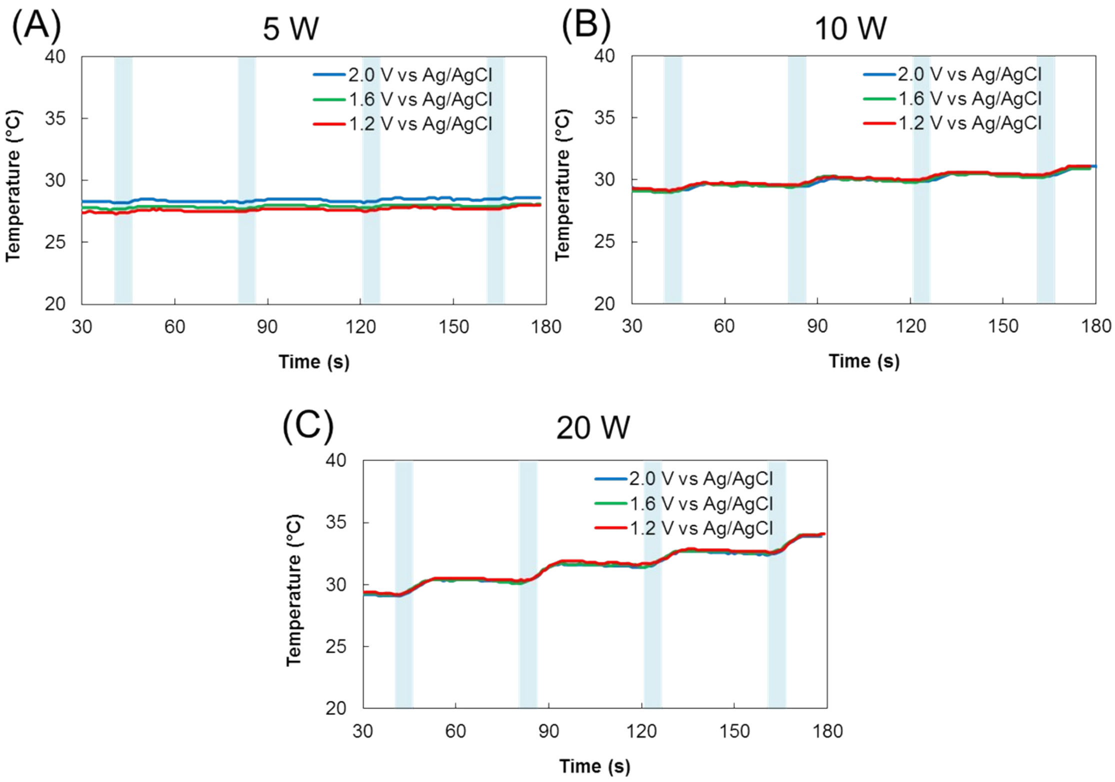

Figure S18. Temperature during application of pulsed RF using 5 mM D_8Ru-POM at (A) 5 W, (B) 10 W and (C) 20 W using designated applied potential of 1.2 to 2.0 V vs Ag/AgCl.